Chapter 1
Introduction

We have seen that there are a lot of experiments designed to reveal neutrino mixing parameters in neutrino oscillation. For three-flavor neutrino oscillation, the Pontecorvo-Maki-Nakagawa-Sakata mixing matrix which transforms the neutrino mass eigenstates $\nu_i\,(i=1,\,2,\,3)$ into flavor eigenstates $\nu_\alpha\,(\alpha = e,\,\mu,\,\tau)$ can be parameterized as

$$\begin{pmatrix} 1 & 0 & 0 \\ 0 & \cos\theta_{23} & \sin\theta_{23} \\ 0 & -\sin\theta_{23} & \cos\theta_{23} \end{pmatrix} \begin{pmatrix} \cos\theta_{13} & 0 & e^{-i\delta_{CP}}\sin\theta_{13} \\ 0 & 1 & 0 \\ -e^{-i\delta_{CP}}\sin\theta_{13} & 0 & \cos\theta_{13} \end{pmatrix} \begin{pmatrix} \cos\theta_{12} & \sin\theta_{12} & 0 \\ -\sin\theta_{12} & \cos\theta_{12} & 0 \\ 0 & 0 & 1 \end{pmatrix}$$

where the first matrix corresponds to atmospheric neutrino oscillation, the second one is responsible for reactor neutrino oscillation, and the last one corresponds to the solar neutrino oscillation. The Super-Kamiokande [1] experiment for atmospheric neutrino gives

$$1.5\times10^{-3}\,\mathrm{eV}^2 < \left|\Delta m^2_{31}\right| < 3.4\times10^{-3}\,\mathrm{eV}^2 \quad , \quad \sin^2 2\theta_{23} > 0.92 \tag{1.1}$$

at 90% C.L. Another result based on L/E analysis in [2] gives

$$1.9\times10^{-3}\,\mathrm{eV}^2 < \left|\Delta m^2_{31}\right| < 3.0\times10^{-3}\,\mathrm{eV}^2 \quad , \quad \sin^2 2\theta_{23} > 0.9 \tag{1.2}$$

where the best-fit values are given by $\sin^2 2\theta_{23} = 1$ and $\Delta m^2_{31} = 2.4\times10^{-3}\,\mathrm{eV}^2$. The atmospheric oscillation is also confirmed by the accelerator based experiment K2K [3]. Similarly, the solar neutrino mixing parameters are also confirmed by the KamLAND experiment [4]. The updated 2σ parameter ranges are [5]

$$7.21\times10^{-5}\,\mathrm{eV}^2 < \left|\Delta m^2_{21}\right| < 8.63\times10^{-5}\,\mathrm{eV}^2 \quad , \quad 0.267 < \sin^2 2\theta_{12} < 0.371 \tag{1.3}$$

The best-fits values are $\sin^2\theta_{12} = 0.314$ and $\Delta m^2_{21} = 7.92\times10^{-5}\,\mathrm{eV}^2$. Moreover, the mixing parameter for reactor neutrino θ_{13} is constrained by the CHOOZ experiment [6] with $\sin^2 2\theta_{13} < 0.1\,(\theta_{13} < 9^\circ)$ for large Δm^2_{31}. Despite the above achievements, the octant of θ_{23} and the sign of Δm^2_{31} are still undetermined.

Furthermore, the CP-violation phase δ_{CP} is also unknown so far. In this thesis, we probe the octant of θ_{23} by combining the appearance oscillation $\nu_e \rightarrow \nu_\mu$ and disappearance

oscillation $\nu_\mu \to \nu_\mu$. We study these oscillation modes at the magic baseline where the effect of CP-violation phase δ_{CP} can be ignored.

This thesis is organized as follows. In chapter 2, we review the neutrino oscillation equations of motion, and give analytic results for oscillation probabilities $\nu_e \to \nu_\mu$ and $\nu_\mu \to \nu_\mu$. We will also define the magic baseline [7] and calculate its value both analytically and numerically. In chapter 3, we present a combined $\nu_e \to \nu_\mu$ and $\nu_\mu \to \nu_\mu$ oscillation analysis for probing the θ_{23} octant in a 20-GeV neutrino factory operated at magic baseline. The effect of CP-violation phase δ_{CP} is shown to be negligible in such a baseline. We conclude in chapter 4.

Chapter 2
Neutrino Oscillation and the Magic Baseline

Neutrino oscillation is a known phenomenon that has been confirmed by many experimental data [2, 3, 4, 8]. It is due to the non-coincidence between neutrino mass eigenstates, $\nu_i\,(i=1,2,3)$, and neutrino flavor eigrnstates, $\nu_\alpha\,(\alpha=e,\mu,\tau)$. These eigenstates are related by Pontecorvo-Maki-Nakagawa-Sakata (PMNS) mixing matrix given by

$$U=\begin{pmatrix} c_{12}c_{13} & s_{12}c_{13} & s_{13}e^{-i\delta_{CP}} \\ -s_{12}c_{23}-c_{12}s_{13}s_{23}e^{i\delta_{CP}} & c_{12}c_{23}-s_{12}s_{13}s_{23}e^{i\delta_{CP}} & c_{13}s_{23} \\ s_{12}s_{23}-c_{12}s_{13}c_{23}e^{i\delta_{CP}} & -c_{12}s_{23}-s_{12}s_{13}c_{23}e^{i\delta_{CP}} & c_{13}c_{23} \end{pmatrix} \tag{2.1}$$

through $\nu_\alpha=\sum_i U_{\alpha i}\nu_i$, where $s_{ij}\equiv\sin\theta_{ij}$ and $c_{ij}\equiv\cos\theta_{ij}$. One can assume that θ_{ij} lies between 0 and π/2 for generality, while CP-violation phase δ_{CP} lies between 0 and 2π. The ratio of neutrinos with different flavors changes during neutrino propagation, and the evolution is governed by the following equation:

$$i\frac{d}{dt}\begin{pmatrix}\nu_e\\ \nu_\mu\\ \nu_\tau\end{pmatrix}=\left\{\frac{1}{2E_\nu}U\begin{pmatrix}0&0&0\\0&\Delta m_{21}^2&0\\0&0&\Delta m_{31}^2\end{pmatrix}U^\dagger+\begin{pmatrix}V(x)&0&0\\0&0&0\\0&0&0\end{pmatrix}\right\}\begin{pmatrix}\nu_e\\ \nu_\mu\\ \nu_\tau\end{pmatrix} \tag{2.2}$$

where $\Delta m_{ij}^2=m_i^2-m_j^2$, mass-squared difference between *i*-th and *j*-th mass eigenstates. Besides, the effective potential $V(x)\equiv\sqrt{2}G_F N_e(x)$ introduces the matter effect arising from the interaction between ν_e and electrons in the medium [9], where $N_e(x)$ is the electron number density, and G_F is the Fermi constant.

2.1 The magic baseline

CP-violation phase δ_{CP} is still an unknown parameter. In order to make a clear measurement of other neutrino oscillation properties, it is necessary to consider the case when the CP-violation phase can be dropped out. In this section, we are going to follow the

discussion in [7]. One will see here that when the baseline length is equal to the integer of refraction length, the solar amplitude A_S in neutrino oscillation probability, which is accompanied with CP-violation phase, becomes zero. In such a case, we can drop out the effect of CP-violation phase by simply setting it to zero.

2.1.1 Where does the magic baseline come from?

One can first rewrite PMNS mixing matrix as $U_{PMNS} = U_{23} I_\delta U_{13} I_{-\delta} U_{12}$ with U_{ij} the rotation matrix performed in *ij*-plane by the angle θ_{ij}, and $I_\delta = diag\ (1, 1, e^{i\delta})$ is the matrix of CP-violation phase. The probability of $\nu_e \rightarrow \nu_\mu$ can then be represented as [7, 10]:

$$P(\nu_e \rightarrow \nu_\mu) = \left|\cos\theta_{23} A_S\, e^{i\delta_{CP}} + \sin\theta_{23} A_A\right|^2 \tag{2.3}$$

where A_S is the solar amplitude depending mainly on Δm^2_{21} and θ_{12}, and A_A is the atmospheric amplitude depending on Δm^2_{31} and θ_{13}. Notice that this is the case expanding up to the lowest order of $\Delta m^2_{21} / \Delta m^2_{31}$ and $\sin^2\theta_{13}$ [11]. With constant density medium profile, which will be discussed in the next section, one can obtain up to a phase factor that

$$A_S = \sin 2\theta^m_{12} \sin\frac{\phi^m_S}{2} \tag{2.4}$$

where θ^m_{12} is the 1-2 mixing angle, and $\varphi^m_S = 2\pi L / l_m$ is the oscillation phase with l_m the oscillation length [12], and L the baseline length. The index m expresses those parameters in matter. One can find that when L is equal to l_m, the solar amplitude A_S vanishes. In this case, the baseline length L is called the magic baseline L_{magic}, since the exact value of δ_{CP} can be neglected at such baseline length. In this way, to find out how long the oscillation length l_m is becomes crucial for the determination of the magic baseline L_{magic}. Further consideration of oscillation length l_m is stated below.

By neglecting the U_{13} transformation matrix in PMNS in equation (2.2), one can first obtain the result [13] as:

$$\Delta m^m_{21} = \sqrt{(\Delta m^2_{21} \sin 2\theta_{12})^2 + (V - \Delta m^2_{21} \cos 2\theta_{12})^2} \tag{2.5}$$

and rewrite the equation with the definition of oscillation length $l = 4\pi E / \Delta m^2_{21}$ [12] as

$$l_m = l\left(\sqrt{\sin^2 2\theta_{12} + (\frac{l}{l_0} - \cos 2\theta_{12})^2}\right)^{-1}. \tag{2.6}$$

where $l_0 = 2\pi / V$. According to equations (2.5) and (2.6), one will obtain $l_m \approx l_0$ if neutrinos travel in the medium with a very large density or carry large energies ($l >> l_0$). The lower

limit of the neutrino energy (0.5 ~ 1GeV) for this equality to hold can be estimated by comparing the value of l and l_0 [7]. The oscillation phase thus becomes

$$\phi_S^m = \frac{2\pi L}{l_0} \tag{2.7}$$

As $L = l_0$, oscillation phase equals to 2π, and the solar amplitude A_S vanishes. This leads to

$$P(\nu_e \to \nu_\mu) \approx \left|\sin\theta_{23} A_A\right|^2. \tag{2.8}$$

The dependence on CP-violation phase and solar neutrino amplitude therefore disappears if the baseline length just equals to l_0. This is the so-called magic baseline.

Furthermore, one can define l_0 as the refraction length, the distance that an additional phase difference ε which neutrinos acquire due to the interaction with matter equals to 2π. That is

$$\varepsilon = V l_0 = 2\pi \tag{2.9}$$

where $V \equiv \sqrt{2} G_F N_e$ is the potential difference for ν_e and ν_μ in the usual matter. In this way, when the baseline length is equal to the integer of refraction length, the effect of CP-violation phase can be dropped out.

2.1.2 Corrections to the magic baseline

Since some approximations have been made in the previous calculation, discussion of corrections due to the negligence of the higher order of $\Delta m_{21}^2 / \Delta m_{31}^2$ and $\sin^2\theta_{13}$ is needed. The first one is due to $l_m \neq l_0$, and another one comes from the dependence of A_S on 1-3 mixing angle. These corrections can be as large as 3%.

Since only the first term of expansion is taken at the $l >> l_0$ limit in last section, we have the following correction from equation (2.7) by taking the second term into account when the limit, $l >> l_0$, is not satisfied perfectly

$$L_{magic} = l_m \approx l_0 \left(1 + \cos 2\theta_{12} \frac{l_0}{l}\right) = l_0 \left(1 + \cos 2\theta_{12} \frac{\Delta m_{21}^2}{2EV}\right) \tag{2.10}$$

One can see that the correction becomes larger with the decrease of neutrino energy or the effective potential.

By considering the explicit calculations of A_S [7], one can perform an additional 1-3 rotation of neutrino basis and make a block-diagonalization of the obtained Hamiltonian. The final modified magic baseline length in [7] is

$$L_{magic} \approx l_0 \left(1 + \cos 2\theta_{12} \frac{l_0}{l} + s_{13}^2 \right) \tag{2.11}$$

We can see that in section 2.1.1, the magic baseline is derived under the assumption that θ_{13} is very small. With corrections in section 2.1.2, the magic baseline equality is still approximately satisfied. In order to obtain a more explicit value of the magic baseline, we will perform numerical calculations in the next chapter.

2.2 The neutrino oscillation probability

To obtain analytic expression for neutrino oscillation probabilities, we introduce an approximation of the earth density profile. For a given medium, one can divide the neutrino propagation length L into several segments with varying densities. If L_i is the length of one segment with ρ_i the corresponding matter density, we can calculate an average density for the total path-length as $\rho = (\rho_1 L_1 + \rho_2 L_2 + \ldots + \rho_n L_n) / L$.

In the same way, the Earth can be categorized mainly into two layers, the Earth mantle and the Earth core. Therefore, its average density is given by $(\rho_m R_m + \rho_c R_c)/L$ if a neutrino passes both mantle and core parts of the Earth. On the other hand, if a neutrino traverses only the Earth mantle, the average density is ρ_m, and L equals to $2R_m$. In the first case, the total path-length L is given by $L = 2R_m + R_c$ with

$$\begin{aligned} R_m &= R\left(\cos\theta_n - \sqrt{\frac{r_c^2}{R^2} - \sin^2\theta_n} \right), \\ R_c &= 2R\sqrt{\frac{r_c^2}{R^2} - \sin^2\theta_n}, \end{aligned} \tag{2.12}$$

where R = 6371 km is the radius of the Earth and r_c = 3480 km is the radius of the Earth core. θ_n is the neutrino incident Nadir angle as shown in Fig. 2.1, and the critical Nadir angle for neutrino passing the Earth core is 33.17° with the corresponding path-length L = 10674 km.

The probability $P_{\mu\mu}(\nu_\mu \to \nu_\mu)$ and $P_{e\mu}(\nu_e \to \nu_\mu)$ are given by [14]:

$$\begin{aligned} P_{\mu\mu} &= \cos^4\theta_{23} + (u^2 + v^2)\sin^4\theta_{23} + 2\cos^2\theta_{23}\sin^2\theta_{23}(u\cos t + v\sin t), \\ P_{e\mu} &= \sin^2\theta_{23}(1 - u^2 - v^2) \end{aligned} \tag{2.13}$$

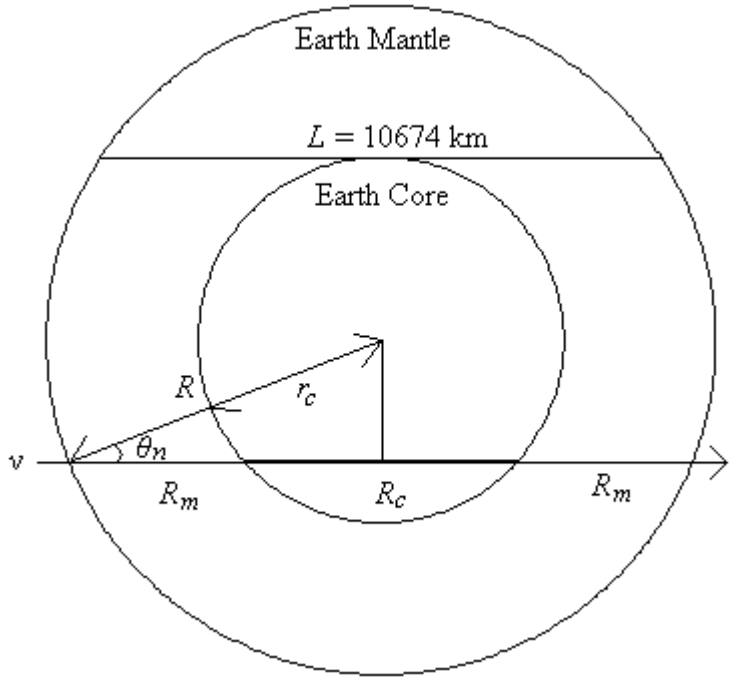

Fig. 2.1 The earth geometric parameters.

where

$$
\begin{aligned}
u &= \cos(2\varphi^m)\cos(\varphi^c) - \cos(2\theta_{13}^c - 2\theta_{13}^m)\sin(2\varphi^m)\sin(\varphi^c), \\
v &= -\cos(2\theta_{13}^m)[\sin(\varphi^c)\cos(2\varphi^m)\cos(2\theta_{13}^c - 2\theta_{13}^m) + \cos(\varphi^c)\sin(2\varphi^m)] \\
&\quad + \sin(2\theta_{13}^m)\sin(\varphi^c)\sin(2\theta_{13}^c - 2\theta_{13}^m),
\end{aligned}
\tag{2.14}
$$

$$
t = \frac{(M_{13}^2)^m + (m_{13}^2)^m}{4E} \times 2L^m + \frac{(M_{13}^2)^c + (m_{13}^2)^c}{4E} \times L^c
$$

with

$$
\begin{aligned}
\phi^{m(c)} &= \frac{\Delta m_{31}^{m(c)}}{4E} L^{m(c)}, \\
(M_{13}^2)^{m(c)} &= (\Delta m_{31}^2 + A_e^{m(c)} + \Delta m_{31}^{m(c)})/2\,, \\
(m_{13}^2)^{m(c)} &= (\Delta m_{31}^2 + A_e^{m(c)} - \Delta m_{31}^{m(c)})/2.
\end{aligned}
$$

Here $\Delta m_{31}^{m(c)}$ is defined as $\sqrt{(\Delta m_{31}^2 \sin 2\theta_{13})^2 + (A_e^{m(c)} - \Delta m_{31}^2 \cos 2\theta_{13})^2}$, and $A_e^{m(c)} = 2\sqrt{2} G_F E N_e^{m(c)}$. The superscripts *m* and *c* here denotes the Earth mantle and the Earth core respectively.

In the following chapter, we will perform a numerical calculation with the approximation of the earth density profile stated above, and see how the obtained magic baseline performs in the determinations of the θ_{23} octant.

Chapter 3
The Dependencies of $P_{e\mu}$ and $P_{\mu\mu}$ on CP-Violation Phases and a Combined Analysis for Determining the θ_{23} Octant

3.1 Quantitative study for dependencies of $P_{e\mu}$ on δ_{CP} and the magic baseline

According to the results in Fig. 3.1 [14], $P_{e\mu}$ is rather sensitive to the CP phase for L = 1000 km and 5000 km, while $P_{\mu\mu}$ is not. Here we are going to study the CP phase dependencies of $P_{e\mu}$ with numerical calculation based on the studies in [14]. Table 3.1 shows the value of oscillation parameters we used here.

For a given baseline length, we can obtain similar results like Fig. 3.1. One can see that, in Fig.3.1, the obvious differences of oscillation probabilities between different CP phases occur at certain energies. To examine the effects of CP phases on muon neutrino appearance probability $P_{e\mu}$, it is useful to find out the maximum and minimum values of $P_{e\mu}$ due to different CP phases in a given energy and baseline length. In this way, we can figure out a specific baseline length where the maximum and minimum values are closest to each other. That is the point where the oscillation probability is most insensitive to the CP-violation phase. It is the so-called magic baseline where we can neglect the effect of δ_{CP} in the calculation by setting $\delta_{CP} = 0$. Since δ_{CP} is still an unknown parameter, knowing this baseline length is useful for our determination of θ_{23} octant.

In this section, we perform calculations in energies between 5 GeV and 20 GeV with a 1-GeV bin size, and calculate the probability $P_{e\mu}$ with baseline length between 0 and the diameter of the earth (largest possible baseline for neutrinos traveling in the earth), 12742 km

	Value used here	Allowed region	Best-fit value
$\cos 2\theta_{23}$	0.2	$\cos^2 2\theta_{23} < 0.1$	0
$\sin^2 \theta_{12}$	0.281	$0.267 < \sin^2 \theta_{12} < 0.371$	0.314
$\sin 2\theta_{13}$	0.2 or 0.3	$\sin^2 2\theta_{13} < 0.1$	
Δm^2_{21}	$8.2\times10^{-5}\ \mathrm{eV}^2$	$7.21\times10^{-5}\ \mathrm{eV}^2 < \Delta m^2_{21} < 8.63\times10^{-5}\ \mathrm{eV}^2$	$7.92\times10^{-5}\ \mathrm{eV}^2$
Δm^2_{31}	$2.4\times10^{-3}\ \mathrm{eV}^2$	$1.9\times10^{-3}\ \mathrm{eV}^2 < \lvert\Delta m^2_{31}\rvert < 3.0\times10^{-3}\ \mathrm{eV}^2$	$2.4\times10^{-3}\ \mathrm{eV}^2$
Y_e	0.5		

Table 3.1 Oscillation parameters used here [9, 14, 15].

with a 1-km bin size. For a given energy and baseline length, we further solve the neutrino oscillation probabilities $P_{e\mu}$ with equation (2.2) for various CP-violation phases between 0 and 2π with a 0.02π bin size. From those probabilities associated with different CP-violation phases, one can find the difference or ratio between the maximum and the minimum ones. Fig. 3.2 ~ Fig. 3.5 show the results. Different colors of lines in Fig. 3.2 ~ Fig. 3.5 represent different energies. The bluer the line is (or the shorter the dashed line is), the higher energy neutrinos have.

Fig. 3.2 (a) shows the numerical calculation of $P_{e\mu}^{\max} - P_{e\mu}^{\min}$. We see that there is a region that all $P_{e\mu}^{\max} - P_{e\mu}^{\min}$ approach zero as we discussed in the beginning of this section. By inspecting Fig. 3.2 (b), the enlarged region of those minimum points in Fig. 3.2 (a), one can see that the baseline length where the minimum difference between $P_{e\mu}^{\max}$ and $P_{e\mu}^{\min}$ occurs are sensitive to neutrino energies. Fig. 3.3 shows the results for $P_{e\mu}^{\min} / P_{e\mu}^{\max}$, and Fig 3.3 (b) displays the baseline points that maximum the ratio of $P_{e\mu}^{\min} / P_{e\mu}^{\max}$ (approaches unity) occurs. The energy dependence of the magic baseline can be easily observed here as well. Fig. 3.4 shows similar graphs with $\sin 2\theta_{13}$ taken to be 0.3. One may see in Fig. 3.4 that the shifting of the magic baseline due to different neutrino energies is much more obvious, which agrees with equation (2.11).

We made both difference and ratio graphs of $P_{e\mu}^{\max}$ and $P_{e\mu}^{\min}$ in Fig.3.2 ~Fig. 3.4. With analysis of the baseline lengths where $P_{e\mu}^{\max}$ is closest to $P_{e\mu}^{\min}$, we obtained Fig. 3.5. In Fig 3.5(a), the magic baseline lengths in low energy are much larger than those in higher energies, which generate a 2.6% difference approximately. The analytic results of equation (2.11) are also plotted in Fig. 3.5 (a), while there is no big difference over energies 5 GeV~20 GeV. Furthermore, in numerical calculations the magic baseline lengths in higher energies decrease about 0.84% when $\sin 2\theta_{13}$ changes from 0.2 to 0.3, while it increases about 1.29% in analytic ones. These differences come from the different definitions of the magic baseline. In comparison with the definition we took in numerical calculation, the one in analytic

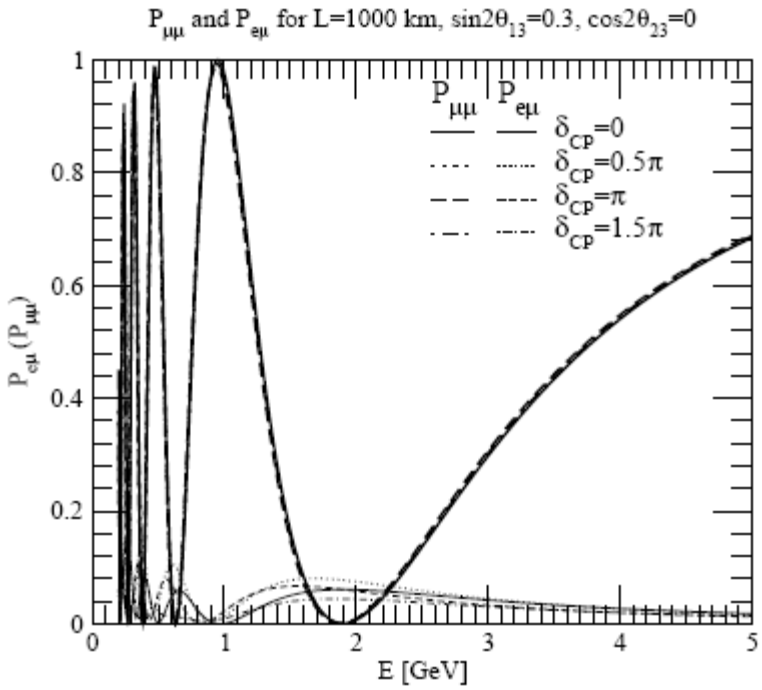

(a)

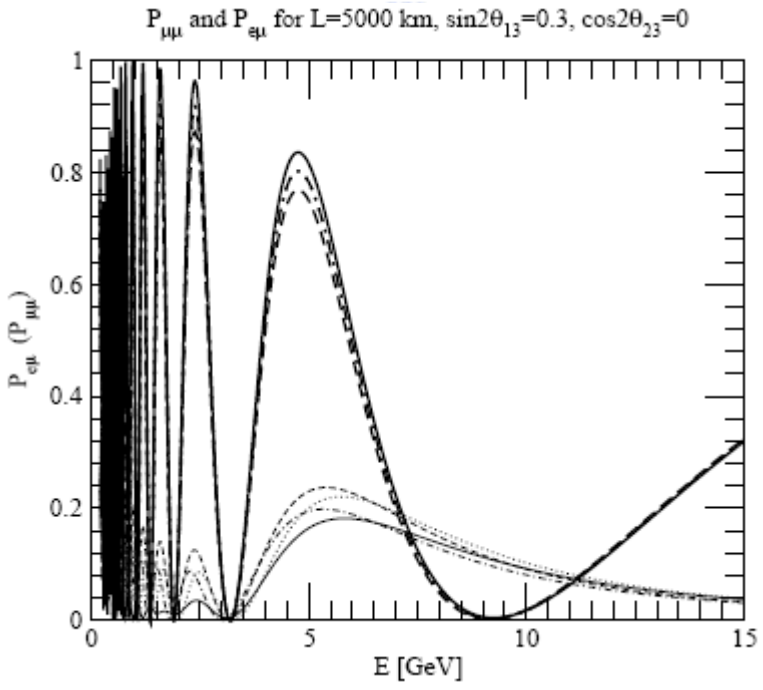

(b)

Fig. 3.1 The CP phase dependencies of $P_{e\mu}$ and $P_{\mu\mu}$ for baseline length L = 1000 km (a) and 5000 km (b) [14].

calculation is defined as the baseline length when the solar amplitude in equation (2.4) equals to zero. One may also notices that the magic baseline obtained here is not perfect, since $P_{e\mu}^{\max} - P_{e\mu}^{\min}$ does not exactly equal to zero, and $P_{e\mu}^{\min} / P_{e\mu}^{\max}$ does not equal to unity at the magic baseline. However, we will see later that this does not influence the results of the determination of θ_{23} octant. We also show numerical results of the magic baseline obtained by different definitions in Fig 3.5 (b). Both sets of $P_{e\mu}^{\max} - P_{e\mu}^{\min}$ and $P_{e\mu}^{\min} / P_{e\mu}^{\max}$ curves match very well, especially for the case $\sin 2\theta_{13} = 0.2$.

From those numerical calculations, we do find a specific baseline length where $P_{e\mu}$ is almost independent of δ_{CP}. However, calculations for different mixing angles and different energies show that the magic baseline length still depends on the mixing angle θ_{13} and neutrinos energy. The difference can be more than 300 km. The shifts are obvious when the energy is below 12 GeV. When the neutrino energy is 20 GeV, the magic baseline is equal to 7513 km when $\sin 2\theta_{13}$ is equal to 0.2, and is equal to 7455 km when $\sin 2\theta_{13}$ changes to be 0.3. We will adopt this result in the next section.

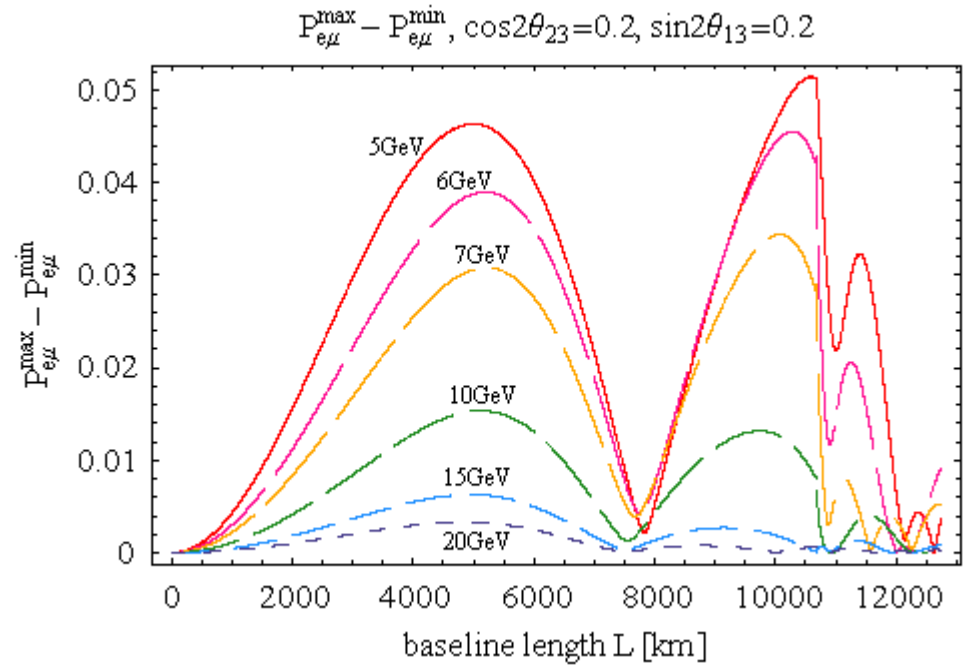

(a)

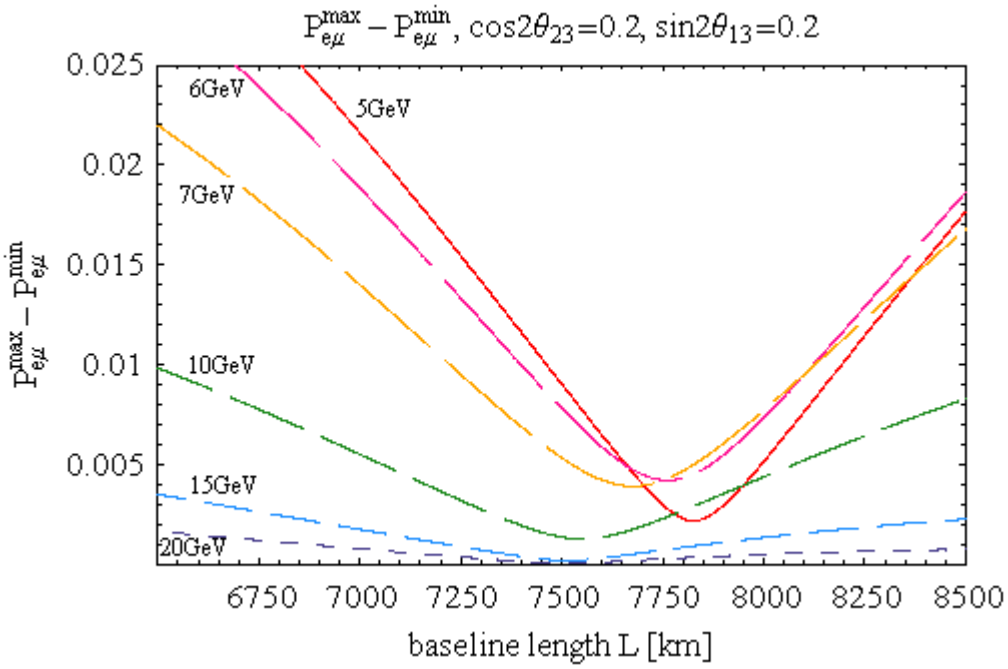

(b)

Fig. 3.2 The difference of $P_{e\mu}^{max}$ and $P_{e\mu}^{min}$ as a function of baseline length for energies 5 GeV (red, solid line), 6 GeV (pink, longest dashed line), 7 GeV (yellow), 10 GeV (green), 15 GeV (blue), and 20 GeV (purple, shortest dashed line). (a) shows the results of entire baseline lengths. (b) shows the results around magic baseline.

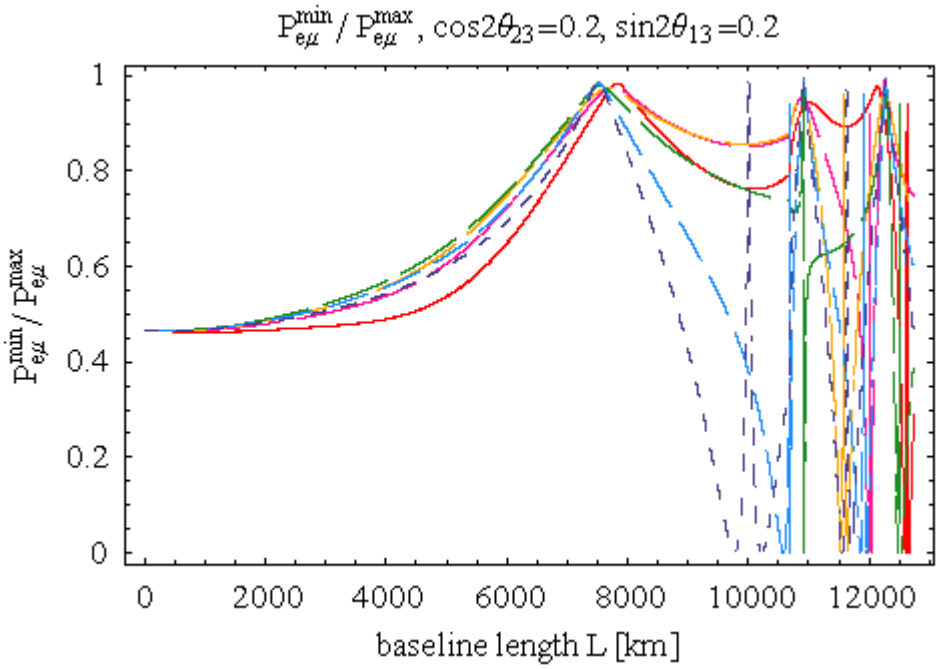

(a)

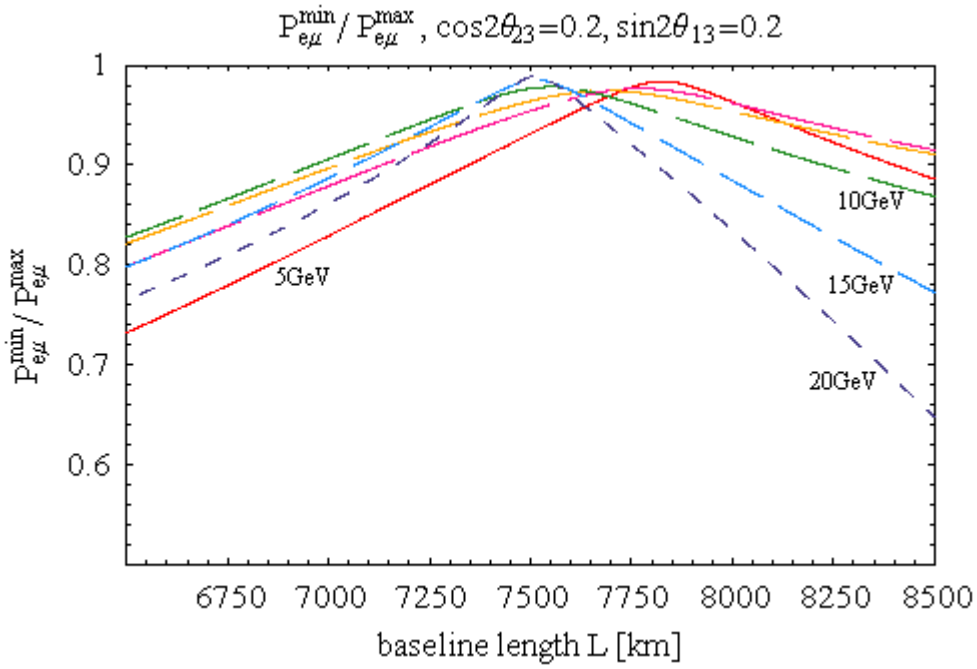

(b)

Fig. 3.3 The ratio of $P_{e\mu}^{max}$ and $P_{e\mu}^{min}$ as a function of baseline length for energies 5 GeV (red, solid line), 6 GeV (pink, longest dashed line), 7 GeV (yellow), 10 GeV (green), 15 GeV (blue), and 20 GeV (purple, shortest dashed line). (a) shows the results of entire baseline lengths. (b) shows the results around magic baseline.

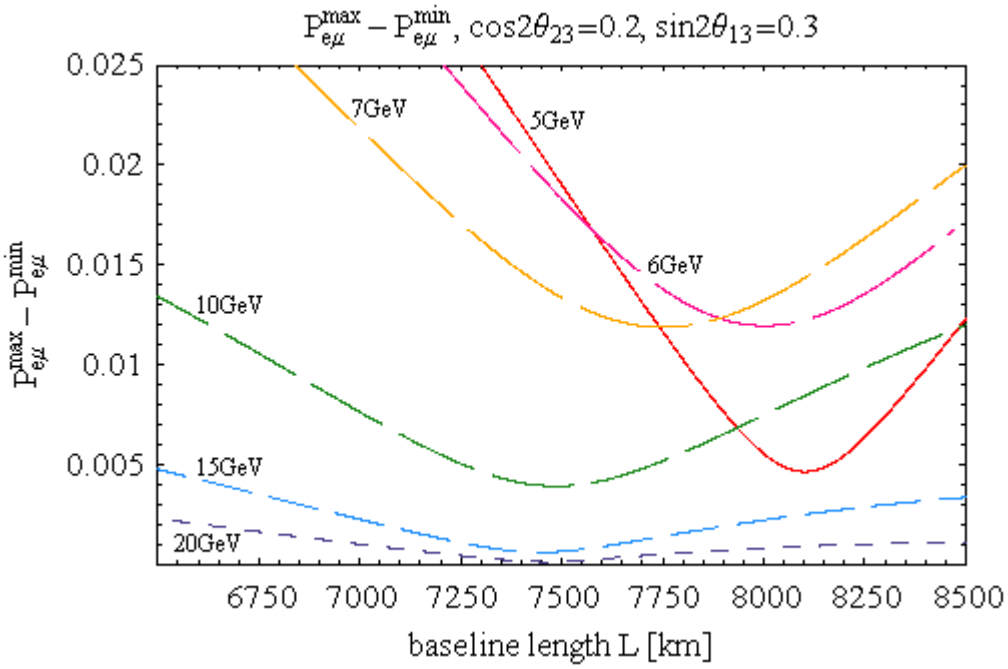

(a)

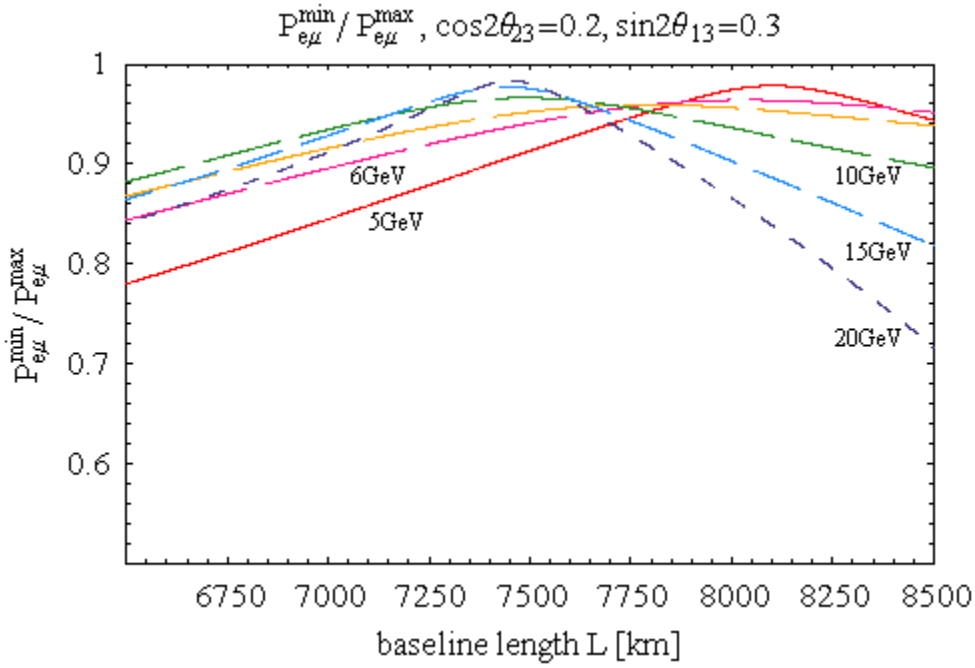

(b)

Fig. 3.4 The difference (a) and the ratio (b) of $P_{e\mu}^{max}$ and $P_{e\mu}^{min}$ as a function of baseline length for energies 5 GeV (red, solid line), 6 GeV (pink, longest dashed line), 7 GeV (yellow), 10 GeV (green), 15 GeV (blue), and 20 GeV (purple, shortest dashed line). Here we take $\sin 2\theta_{13} = 0.3$.

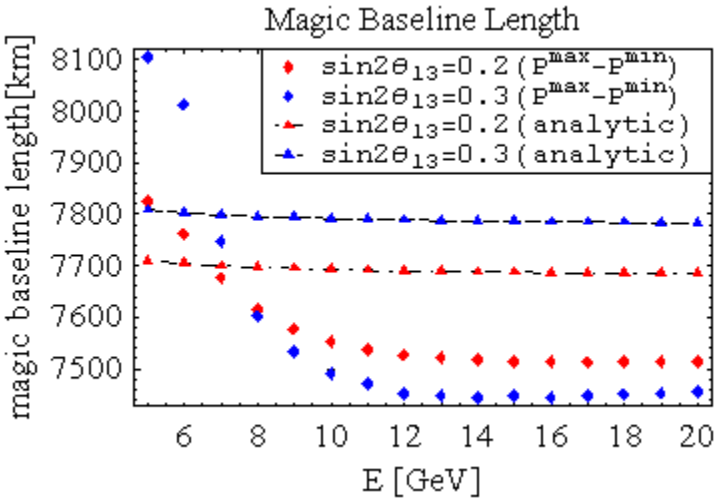

(a)

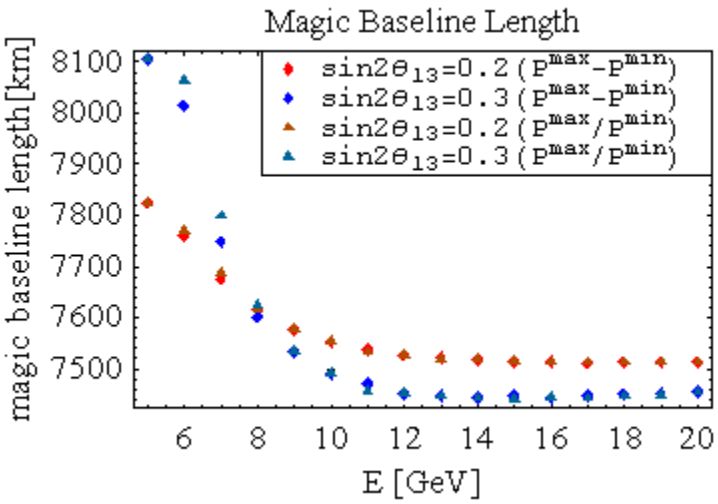

(b)

Fig. 3.5 Magic baseline lengths as a function of energy for both $\sin 2\theta_{13} = 0.2$ and 0.3 in numerical (both $P_{e\mu}^{\max}$ - $P_{e\mu}^{\min}$ and $P_{e\mu}^{\min}$ / $P_{e\mu}^{\max}$ cases) and analytic calculations.

3.2 Combined analysis of appearance and disappearance modes at the magic baseline

3.2.1 The breaking of θ_{23} degeneracy

Other than the CP-violation phase dependencies of $P_{e\mu}$ studied in the last section, we further take a look at θ_{23} and θ_{13} dependencies of $P_{e\mu}$ and $P_{\mu\mu}$. It is instructive to rewrite equation (2.13) into

$$\begin{aligned} P_{\mu\mu} &= f(y,z) = -\alpha y^2 + (\alpha+\beta)y + (1-\beta) \\ P_{e\mu} &= g(y,z) = -\gamma(y-1) \end{aligned} \tag{3.1}$$

where $y \equiv \cos 2\theta_{23}$ and $z \equiv \sin 2\theta_{13}$ with

$$\begin{aligned} \alpha &= -\frac{1}{4}[(u-\cos t)^2 + (v-\sin t)^2], \\ \beta &= \frac{1}{2}(1-u^2-v^2) + \frac{1}{4}[(u-\cos t)^2 + (v-\sin t)^2] \\ \gamma &= \frac{1}{2}(1-u^2-v^2) = \alpha+\beta \end{aligned} \tag{3.2}$$

u and v are defined in (2.14). Note that these results are valid under the condition with $\Delta m^2_{21} / \Delta m^2_{31} = 0$. One can see in equation (3.1) that the θ_{23} degeneracy is broken in both $P_{e\mu}$ and $P_{\mu\mu}$ due to terms linear in y. Hence they are independent of the CP-violation phase δ_{CP}. The effect of the linear term is determined by $\alpha + \beta$, and it becomes obvious when the baseline length is longer than 7000 km [14]. In this way, it is instructive to choose magic baseline (around 7500 ~7600 km) as the baseline length for probing the octant of θ_{23}. In the following sections, we are going to see if θ_{23} degeneracy can be broken with a 20-GeV neutrino factory.

3.2.2 Framework of combined analysis

It has been mentioned before that the solar neutrino amplitude disappears when the baseline length equals to the integer multiple of refraction length:

$$L_{magic} = \frac{2\pi n}{\sqrt{2} G_F N_e} \tag{3.3}$$

In such a case, the effect of δ_{CP} can be ignored. Here we take the shortest baseline length by choosing n = 1, and obtain:

$$\langle N_e \rangle L = \int N_e dL = \frac{\sqrt{2}\pi}{G_F N_e} = 16257 \text{ km} \tag{3.2}$$

Given the earth density profile, one obtains $L \approx 7600$ km [13]. We will first illustrate the framework of the combined analysis in a neutrino factory and show the results in [15] where δ_{CP} is set to be zero at baseline length 7600 km.

A neutrino factory produces electron neutrino and anti-neutrino beams through the following muon decay processes:

$$\mu^+ \to \overline{\nu_\mu} + e^+ + \nu_e$$
$$\mu^- \to \nu_\mu + e^- + \overline{\nu_e}$$

and detect the muons generated from final neutrinos after propagating a baseline. The detector mass is of the order kilotons. The differential event rates for $\nu_i \to \nu_f$ can be written as

$$\frac{dn_{i\to f}}{dE'} = N \int dE \times \phi_i(E) \times P_{\nu_i \to \nu_f}(E) \times \sigma_{\nu_f}(E) \times R_f(E, E') \times \varepsilon_f(E') \tag{3.3}$$

where E is the incident neutrino energy, E' is the reconstructed neutrino detected energy, ϕ_i is the incident neutrino flux, $P_{\nu_i \to \nu_f}$ is the oscillation probability form flavor i to flavor j, σ_{ν_f} is the ν_f- nucleon scattering cross section, R_f is the energy resolution function, ε_f is the detection efficiency of ν_f, and N is the normalization constant given by

$$N = n_y \times 10^9 \times N_A \times M_d \tag{3.4}$$

where n_y is the running years of this experiment, N_A is the Avogadro's number, and M_d is the detector mass in kilotons. In this work, n_y is taken to be 4 years for both μ^+ and μ^- modes, and $M_d = 50$. The initial ν_e of appearance mode $\nu_e \to \nu_\mu$ arises from the μ^+ decay, while the initial ν_μ of appearance mode $\nu_\mu \to \nu_\mu$ comes from the μ^- decay. Their expected fluxes in this work are given by [16]

$$\phi_i(E) = \left(\frac{N_\mu E_\mu}{\pi m_\mu^2 L} \right) g_i(E / E_\mu) \tag{3.5}$$

where N_μ is the number of muon decays per year with $x \equiv E / E_\mu$, $g_{\nu_e}(x)$ $= g_{\bar{\nu}_e}(x) = 12x^2(1-x)$, $g_{\nu_\mu}(x) = g_{\bar{\nu}_\mu}(x) = 2x^2(3-2x)$, $E_\mu = 20$GeV, $L = 7600$ km. We take $N_{\mu^+} = N_{\mu^-} = 5 \times 10^{20}$ as discussed in [17]. The energy resolution function R_f is represented in Gaussian form as

$$R_f(E, E') = \frac{1}{\sqrt{2\pi\lambda_f^2}} \exp\left[-\frac{(E - E')^2}{2\lambda_f^2} \right] \tag{3.6}$$

The Gaussian width λ_f is taken to be $0.15E$ for either ν_μ or $\bar{\nu}_\mu$, the final states we are interested. The detection efficiency ε_f for these final states is given by

$$\varepsilon_f(E') = \frac{\eta_f}{4}\left(\frac{E'}{4} - 1\right) \tag{3.7}$$

where the efficiency factor η_f is 0.35 for oscillation mode $\nu_e \rightarrow \nu_\mu$ and $\bar{\nu}_\mu \rightarrow \bar{\nu}_\mu$, while it is 0.45 for $\bar{\nu}_e \rightarrow \bar{\nu}_\mu$ and $\nu_\mu \rightarrow \nu_\mu$ [17]. The last parameter, ν_f- nucleon scattering cross section, is equal to $(0.677 \pm 0.014) \times 10^{-38} E$ cm^2/GeV for muon neutrino and is equal to $(0.34 \pm 0.020) \times 10^{-38} E$ cm^2/GeV for anti-muon neutrino [18] [19].

With equation (3.3), neutrino mixing parameters mentioned in Table 3.1 can be input for generating a simulated ν_μ spectra from 5 GeV to 20 GeV with a 1-GeV bin size. Here we take $\sin 2\theta_{13} = 0.2$, and perform the combined analysis in normal hierarchy $\Delta m^2_{31} > 0$. By determining the 2σ and 3σ contours of mixing parameters θ_{23} and Δm^2_{31}, we are able to see how the θ_{23} degeneracy is lifted by the combined analysis of muon neutrino appearance and disappearance modes. The χ^2-function of the fit is given by [20]

$$\chi^2 = \sum_{i=1}^{n}\left(\left[2\langle x_i\rangle - x_i\right] + 2x_i \ln\frac{x_i}{\langle x_i\rangle}\right) \tag{3.8}$$

where n is the numbers of bins, x_i is the number of events in i-th bin, while $\langle x_i\rangle$ is the expected number of events in i-th bin calculated by the input best-fit parameters in Table 3.1. The left panel of Fig. 3.6 shows the contours for both appearance and disappearance modes. One can see that the fitting to the disappearance mode results in two small regions, while the fitting to

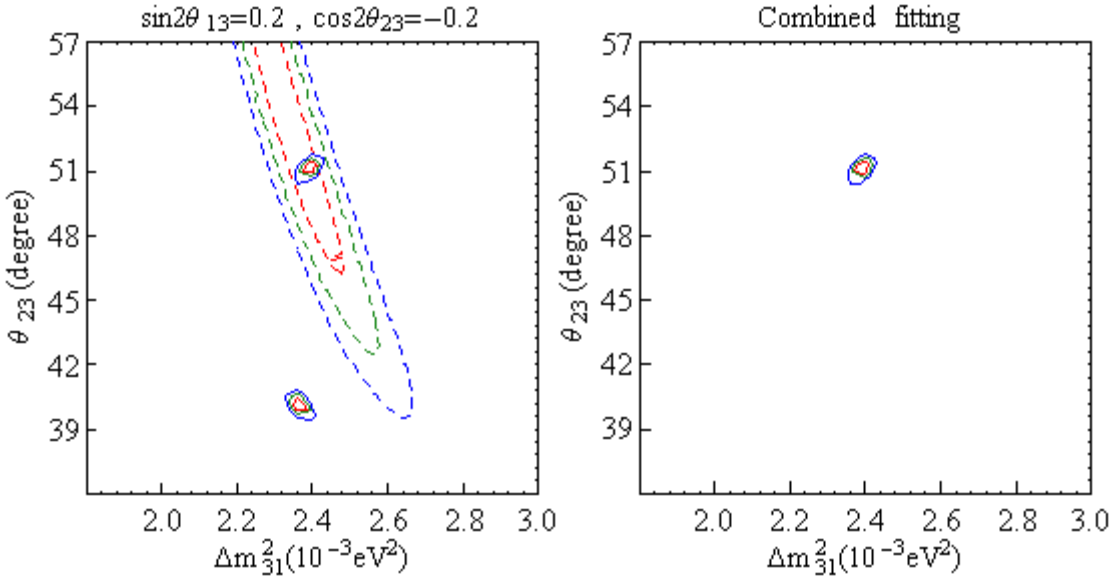

Fig. 3.6 The 1σ (red), 2σ (green), and 3σ (blue) contours for ranges of neutrino mixing parameters θ_{23} and Δm^2_{31} for $\sin 2\theta_{13} = 0.2$, and the input values $\theta_{23} = 50.768^\circ$ and $\Delta m^2_{31} = 2.4 \times 10^{-3}$ (eV^2). The dashed lines come from the analysis of appearance mode $P_{e\mu}$, and the solid lines come from disappearance mode $P_{\mu\mu}$ for 20-GeV neutrinos.

the appearance mode results in a larger area due to a low statistics. By combining both fittings, the θ_{23} degeneracy is lifted. The best-fit point is located at θ_{23} = 51.8 ° and $\Delta m^2_{31} = 2.33\times10^{-3}\,(\mathrm{eV}^2)$, which also coincides well with input values, θ_{23} = 50.77 ° and $\Delta m^2_{31} = 2.4\times10^{-3}\,(\mathrm{eV}^2)$. It is instructive to see that the appearance and disappearance modes complement each other well. In this case, if one can measure $P_{e\mu}$ and $P_{\mu\mu}$ with enough statistics, it is possible to resolve the octant of θ_{23}. More studies of 20-GeV neutrino factory for resolving θ_{23} octant can be found in [15].

3.2.3 The combined analysis at different CP-violation phases

So far only the case of CP-violation phase δ_{CP} = 0 has been calculated at the magic baseline, 7600 km. In this subsection, we will perform the combined analysis for other CP-violation phases as well. Table 3.2 shows some best-fit points obtained both in muon neutrino appearance and disappearance modes and the ones after the combined fitting. In order to find out how CP-violation phases affect best-fit points at the magic baseline, we first assume that the real CP-violation phase value is equal to zero. Furthermore, we input the other different CP-violation phase (wrong CP phases) values while performing the χ^2-function fitting. In this way, we can see that whether we still perform this fitting well or not even if we make a wrong guess of the CP-violation phase. One can clearly see in the Table 3.2 that the obtained best-fit points do not change much as we change the CP-violation phase. Note that we list two best-fit points for each octant of θ_{23} in $P_{\mu\mu}$ mode.

We can see that the best-fit points of Δm^2_{31} do not change significantly like θ_{23}. Large fluctuations of θ_{23} are due to the low statistics of appearance mode $P_{e\mu}$. One can see in

	$P_{e\mu}$		$P_{\mu\mu}$		Combined fitting	
δ_{CP}	θ_{23}	$\Delta m^2_{31}(\times10^{-3})$	θ_{23}	$\Delta m^2_{31}(\times10^{-3})$	θ_{23}	$\Delta m^2_{31}(\times10^{-3})$
0	43.567	2.56	40.1061 50.7685	2.4	50.7685	2.4
$\frac{3\pi}{7}$	43.8538	2.56	40.1061 50.4764	2.4	50.4764	2.4
$\frac{8\pi}{7}$	43.2801	2.56	39.8185 50.4764	2.4	50.4764	2.4
$\frac{12\pi}{7}$	43.2801	2.56	40.1061 50.7685	2.4	50.7685	2.4

Table 3.2 Best-fit points calculated through various CP-violation phases at magic baseline with input values $\theta_{23} = 50.768°$ and $\Delta m^2_{31} = 2.4\times10^{-3}(\mathrm{eV}^2)$.

Fig. 3.6 that contours for allowed Δm^2_{31} values do not stretch widely as contours for allowed θ_{23} do. Finally, it is reasonable to set CP-phase to zero in the first place at the magic baseline. The result for the combined fitting always falls into the correct octant.

In the case that the input value of θ_{23} changes into $39.232°$, the fitting still goes very well. The results are shown in Fig. 3.7 and Table 3.3, and the best-fit point came out in a similar value with the input one. Furthermore, we also performed the analysis at the magic baseline

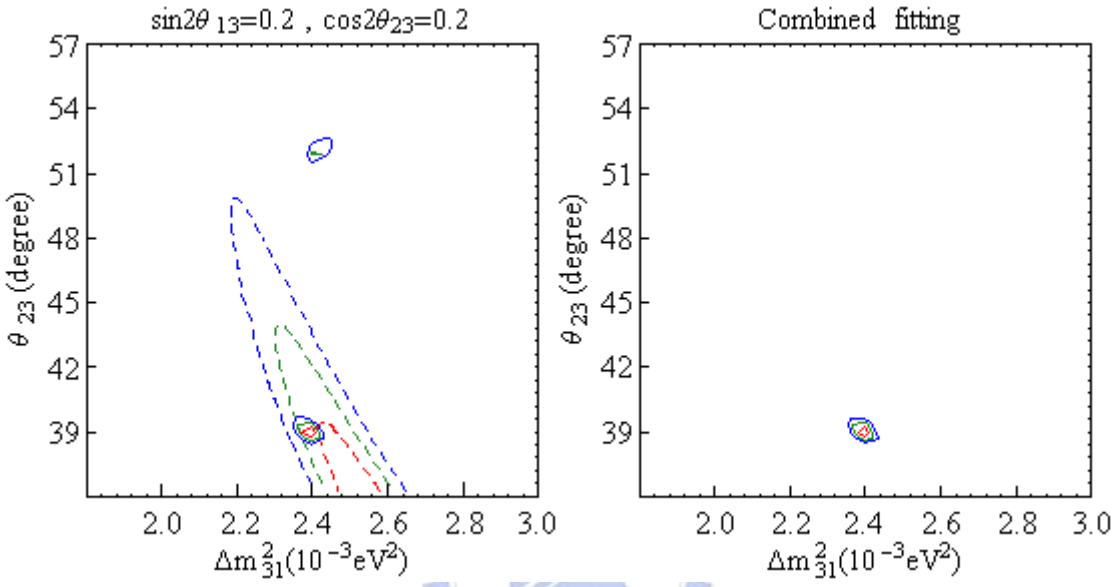

Fig. 3.7 The 1σ (red), 2σ (green), and 3σ (blue) contours for ranges of neutrino mixing parameters θ_{23} and Δm^2_{31} for $\sin 2\theta_{13} = 0.2$, and the input values $\theta_{23} = 39.232^\circ$ and $\Delta m^2_{31} = 2.4\times10^{-3}\,(\mathrm{eV}^2)$. The dashed lines come from the analysis of appearance mode $P_{e\mu}$, and the solid lines come from disappearance mode $P_{\mu\mu}$ for a 20-GeV neutrino factory.

	$P_{e\mu}$		$P_{\mu\mu}$		Combined fitting	
δ_{CP}	θ_{23}	$\Delta m^2_{31}(\times10^{-3})$	θ_{23}	$\Delta m^2_{31}(\times10^{-3})$	θ_{23}	$\Delta m^2_{31}(\times10^{-3})$
0	36.571	2.44	38.9388 51.9433	2.4	38.9388	2.4
$\frac{3\pi}{7}$	36.8699	2.44	38.6455 51.9433	2.4	38.6455	2.4
$\frac{8\pi}{7}$	36.571	2.44	38.6455 51.6485	2.4	38.6455	2.4
$\frac{12\pi}{7}$	36.571	2.44	38.9388 51.9433	2.4	38.9388	2.4

Table 3.3 Best-fit points calculated through various CP-violation phases at the magic baseline with input values $\theta_{23} = 39.232°$ and $\Delta m^2_{31} = 2.4\times10^{-3}(\mathrm{eV}^2)$.

L = 7513 km which we obtained with the numerical calculation. The results are shown in Table 3.4. Once again, the fitting goes very well, which indicates that the possible magic baseline length can vary for several kilometers.

	$P_{e\mu}$		$P_{\mu\mu}$		Combined fitting	
δ_{CP}	θ_{23}	$\Delta m^2_{31}(\times 10^{-3})$	θ_{23}	$\Delta m^2_{31}(\times 10^{-3})$	θ_{23}	$\Delta m^2_{31}(\times 10^{-3})$
0	48.1577	2.44	40.3966	2.4	50.7685	2.44
			50.7685	2.44		
$\frac{3\pi}{7}$	47.8696	2.44	40.3966	2.4	50.7685	2.44
			50.7685	2.44		
$\frac{8\pi}{7}$	47.5818	2.44	40.1061	2.4	50.4764	2.44
			50.4764	2.44		
$\frac{12\pi}{7}$	47.8696	2.44	40.3966	2.4	50.7685	2.44
			50.7685	2.44		

Table 3.4 Combined analysis of muon neutrino appearance and disappearance modes at baseline length L = 7513 km with input values $\theta_{23} = 50.768°$ and $\Delta m^2_{31} = 2.4\times 10^{-3}(\text{eV}^2)$.

Chapter 4
Summary and Conclusion

We can see from this work that even we know nothing about the CP-violation phase, it is still possible to probe neutrino mixing parameters at the magic baseline. The analytic value of magic baseline is first defined and derived in Chapter 2, and we also adopt this magic baseline L_{magic} = 7600 km in the analysis with respect to the muon neutrino appearance and disappearance modes. Furthermore, we consider some possible corrections to the approximations used in deriving the magic baseline, and found that the magic baseline lengths can vary with different neutrino energies if the neutrino energy is smaller than 1GeV. The value of $\sin 2\theta_{13}$ also affects the value of magic baseline. However, θ_{13} is only constrained to be $\sin^2 2\theta_{13} < 0.1 (\theta_{13} < 9^\circ)$.

We also determine the magic baseline numerically. We calculate both the cases of $\sin 2\theta_{13}$ = 0.2 and 0.3 to see how $\sin 2\theta_{13}$ affects magic baseline length, and we also scan through the energies between 5 GeV and 20 GeV. The results show that there is not much difference between the cases of $\sin 2\theta_{13}$ = 0.2 and 0.3. However, the effect due to the energy difference is up to several hundred kilometers. This becomes obvious especially when the neutrino energy is smaller than 12 GeV. Stable values for larger energies are also different from the analytic results L_{magic} = 7600 km. To verify how these magic baseline lengths can be useful for extracting neutrino oscillation parameters, we performed a combined neutrino oscillation analysis of muon neutrino appearance and disappearance modes.

By following the combined analysis of appearance and disappearance modes in [15], which considers oscillations at the magic baseline L_{magic} = 7600 km and set the effect of CP-violation phase to zero, here we calculate as well the cases when the CP-violation phases equals to $3\pi / 7$, $8\pi / 7$ and $12\pi / 7$. Results come out quite independent of the CP-violation phase, which confirms that there is no need to consider the CP-violation phase at this specific magic baseline. We also see in this combined analysis of muon neutrino appearance and disappearance modes that the best-fit values of θ_{23} and Δm^2_{31} coincide well with the input ones. It shows that a 20-GeV neutrino factory running over 4 years for each of μ^+ and μ^- modes accompanied with a 50-kiloton detector provides enough statistics for resolving these parameters. In this analysis, we also take the magic baseline to be 7513 km which is obtained numerically.

Bibliography

[1] Y. Ashie *et al*. [Super-Kamiokande Collaboration], Phys. Rev. D **71**, 112005 (2005) [arViv:hep-ex/0501064]

[2] Y. Ashie *et al*. [Super-Kamiokande Collaboration], Phys. Rev. Lett. **93**, (2004) 101801 [arViv:hep-ex/0404034]

[3] M.H. Ahn *et al*.[K2K collaboration] Phys Rev. Lett. **93**, (2004) 051801 [arXiv:hep-ex/0402017]

[4] K. Eguchi *et al*. [KamLAND Collaboration]. Phys. Rev. Lett. **90**, (2003) 021802 [arXiv:hep-ex/0212021]

[5] G. L. Fogli, E. Lisi, A. Marrone and A. Palazzo, Prog. Part. Nucl. Phys. **57**, 742 (2006) [arXiv:hep-ph/0506083]

[6] M. Apollonio *et al*. [CHOOZE Collaboration], Phys. Lett. B **466**, 415 (1999) [arXiv:hep-ex/9907037]

[7] A. Y. Smirnov, [arXiv:hep-ph/0610198]

[8] Q. R. Ahmad *et al*. [SNO Collaboration], Phys. Rev. Lett. **89**, 011302 (2002) [arXiv:nucl-ex/0204009]

[9] Y. C. Hsu, *Master Thesis*, NCTU (2005)

[10] Evgeny Kh. Akhmedov *et al*. JHEP **06** (2008) 072 [arXiv:hep-ph/0804.1466]

[11] Evgeny Kh. Akhmedov *et al*. JHEP **0404** (2004) 078 [arXiv:hep-ph/0402175]

[12] Y. L. Tasi, *Master Thesis*, NCTU (2004)

[13] V. Barger, D. Marfatia and K.Whisnant, Phys Rev. D **65**, (2002) 073023 [arXiv:hep-ph/0112119]

[14] G. L Lin, Y. Umeda [arXiv:hep-ph/0612309]

[15] G. L Lin, Y. Umeda Probing the octant of θ_{23} in 20-GeV neutrino factories, submitted to EPJ C.

[16] S. Geer, Phys. Rev. D **57**, (1998) 6989 [Erratum-ibid. D **59**, (1999) 039903] [arXiv:hep-ph9712290]

[17] P. Huber, M. Lindner and W. Winter, Nucl. Phys. B **645**, (2002) 3 [arXiv:hep-ph/0204352]

[18] F. Boehm and P. Vogel, *Physics of Massive Neutrinos* (Cambridge University Press, Cambridge, England, 1987)

[19] J. M. Conrad, M. H. Shaevitz and T. Bolton, Rev. Mod. Phys. **70** (1998) 1341

[20] W. M. Yao *et al*. [Particle Data Group], J. Phys. G **33**, (2006) 1.